



PAPER

[View Article Online](#)
[View Journal](#) | [View Issue](#)Cite this: *Dalton Trans.*, 2025, **54**,
13642

A mitochondria-targeted iridium complex activates anti-tumour immunity by regulating zinc homeostasis in cancer cells and macrophages

Jun-Jian Lu,[†] Xi-Song Feng,[†] Yu Liu, Wan-Di Cao, Zong-Wan Mao * and
Qian Cao *

Intracellular zinc homeostasis and subcellular compartmentalization are exquisitely regulated, playing critical roles in immune regulation, such as inducing inflammatory programmed cell death, producing high levels of interferons and inflammatory cytokines, controlling the polarization and function of macrophages, etc. Herein, we designed two cyclometalated Ir(III) complexes with moderate zinc ion (Zn^{2+}) affinity, capable of re-distributing the endogenous Zn^{2+} from the cytoplasm and vesicles to mitochondria as indicated by ICP-MS measurement, thus inducing mitochondrial dysfunction and apoptosis. Moreover, mitochondria-targeted **Ir2** also displayed better immunoregulation activity than lysosome-targeted **Ir1**, capable of triggering GSDMD-mediated pyroptosis *via* caspase-1 dependent pathway and down-regulating PD-L1 levels in cancer cells. In macrophages, **Ir2** also re-distributed intracellular zinc effectively, leading to an increased zinc level in mitochondria and promoting the M0-to-M1 polarization of macrophages. The antitumor efficacy and immunoregulation activity were also verified *in vivo*. This work suggested that the modulation of endogenous zinc homeostasis both in cancer cells and immune cells would be a promising strategy for activating anti-tumour immunity, and provided new clues for designing novel metallodrugs for cancer chemo-immunotherapy.

Received 5th May 2025,
Accepted 7th August 2025

DOI: 10.1039/d5dt01045d

rsc.li/dalton

Introduction

Zinc is the second most abundant transition metal element in the human body, and its intracellular homeostasis and distribution are exquisitely regulated, playing critical roles in physiological and pathological processes.¹ Most zinc ions (Zn^{2+}) are bound to proteins and enzymes to maintain their structures and stabilities, resulting in a low concentration of free Zn^{2+} in cytoplasm or sequestration in organelles and vesicles.² Intracellular Zn^{2+} is also indispensable for many key cellular processes, such as signal transduction, cellular metabolism, cytoskeleton assembly, immune regulation, and so on.³ For example, Zn^{2+} constitutes metallothionein (MT),⁴ which is responsible for not only cellular Zn^{2+} buffering and storage but also maintaining cellular redox balance, thus participating in the maintenance of both zinc homeostasis and redox homeostasis. Zn^{2+} overload can lead to mitochondrial dysfunction, indirectly causing oxidative stress through the leakage of electrons from aerobic respiration in mitochondria, resulting in mitochondrial DNA (mtDNA) damage and production of

high levels of interferons and inflammatory cytokines.⁵ Meanwhile, Zn^{2+} is a cofactor in zinc finger motifs and proteins involved in DNA repair,^{6,7} thus greatly affecting the DNA damage mediated cellular death process. Zn^{2+} also plays key roles in immune regulation, such as controlling the polarization and function of macrophages,^{8–10} decreasing the integrity of the plasma membrane to trigger the exposure of many damage-associated molecular patterns (DAMP), and inducing cancer cell pyroptosis *via* GSDMD- and GSDME-dependent pathways, which can eventually activate a powerful antitumour immunity.¹¹ Macrophages are integral parts of the innate immune system, classified into the M1 phenotype with tumouricidal activity and the M2 phenotype with immunosuppressive activity.^{12–14} Recent studies have found that zinc supplementation can promote M0-to-M1 polarization of macrophages and strongly inhibit M2 polarization.⁹ Thus, regulating intracellular zinc homeostasis and distribution would be a promising strategy for antitumour therapy and antitumour immunomodulation.

With the rise of metalloimmunology, not only endogenous but also exogenous metal ions and metallodrugs have attracted extensive attention.^{15–19} Several nanomedicines containing zinc have been developed, and they can effectively elicit immune responses *via* immunogenic cell death (ICD),^{20,21} activation of the cyclic GMP-AMP synthase-stimulator of the inter-

MOE Key Laboratory of Bioinorganic and Synthetic Chemistry, School of Chemistry, Sun Yat-Sen University, Guangzhou 510275, China.
E-mail: cesmzw@mail.sysu.edu.cn, caoqian3@mail.sysu.edu.cn

[†]These authors contributed equally to this work.

feron gene signalling pathway,²² inducing pyroptosis,^{23,24} *etc.* However, these functions mainly interfere with zinc homeostasis in cancer cells *via* massive input of exogenous zinc ions. For example, the pH-sensitive zeolitic imidazolate framework-8 can release Zn²⁺ ions in lysosomes, leading to sudden surge of Zn²⁺ in cancer cells, eventually inducing pyroptosis, necrosis and ICD simultaneously for highly efficient activation of anti-tumour immunity.²⁴ By comparison, metallodrugs can regulate zinc homeostasis by interfering with intracellular zinc distribution rather than input of exogenous zinc ions from cellular media or serum. Our group has recently reported a cyclometalated Pt^{IV}-terthiophene complex, which induces the dysregulation of Zn²⁺ transporters and buffering proteins (MT), leading to excess accumulation of Zn²⁺ in cytoplasm, eventually inducing pyroptosis *via* a caspase-1/gasdermin D (GSDMD) pathway and effectively activating antitumour immunity.²⁵ This inspires further development of novel metallodrugs that can regulate zinc homeostasis for antitumour immunomodulation. Iridium(III)-based anticancer complexes have been extensively investigated due to their easily modified ligands,²⁶ subcellular organelle-targeting ability,²⁷ potent anticancer activity and favorable photophysical characteristics,²⁸ meanwhile, Ir(III) complexes can activate antitumour immune response by manipulating the cell death pathways,²⁹ immune checkpoint,³⁰ immunosuppressive microenvironment,^{31,32} *etc.*

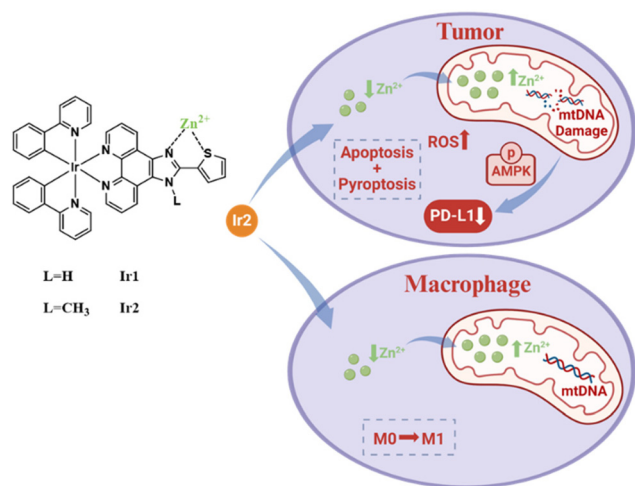
Inspired by these, we rationally designed two cyclometalated Ir(III) complexes (**Ir1**/**Ir2**) with a thiophene sulfur donor and an imidazole nitrogen donor on their ligands, which could provide moderate Zn²⁺ affinity (Scheme 1). After entering cancer cells, **Ir1** and **Ir2** accumulate in lysosomes and mitochondria, respectively, but both could effectively promote the redistribution of zinc from cytoplasm to mitochondria, and **Ir2** had a more pronounced effect. The elevated zinc levels in mitochondria contrib-

uted to mitochondrial dysfunction as indicated by mitochondrial DNA (mtDNA) damage, mitochondrial membrane potential (MMP) loss, and phosphorylation of adenosine 5'-monophosphate-activated protein kinase (AMPK), eventually inducing GSDMD mediated pyroptosis and AMPK mediated programmed cell death 1 ligand 1 (PD-L1) down-regulation. Meanwhile, **Ir2** also induced the excess accumulation of Zn²⁺ in the mitochondria of macrophages accompanied by a decrease in the cytoplasm, leading to the polarization of macrophages from the M0 to M1 phenotype. As is well known, induction of pyroptosis, polarization of M1 macrophages, and down-regulation of PD-L1 are all effective means of activating immunity; therefore, mitochondria targeted **Ir2** has shown great potential in cancer chemotherapeutic *via* regulating intracellular zinc distribution/homeostasis.

Results and discussion

Synthesis, characterization and Zn²⁺ binding properties

As shown in Scheme S1, **Ir1** and **Ir2** were synthesized by separately reacting two thiophene-containing ligands (**L1**–**L2**) with a chloro-bridged Ir(III) dimer followed by anion exchange with KPF₆. The related metal complex **Ir3** containing similar ligands without a Zn²⁺ binding moiety was also synthesized following literature methods for comparison.³³ All complexes were purified by column chromatography and characterized by ESI-MS, ¹H NMR and ¹³C NMR (Fig. S1–S8, SI). HPLC was used to determine the purity of complexes, and **Ir1**/**Ir2** showed purity greater than 98% (Fig. S9, SI). The UV-Vis spectra of **Ir1**/**Ir2** in PBS, CH₃CN, and CH₂Cl₂, exhibited similar absorptions attributed to intraligand π – π^* transitions (250–350 nm) and metal-to-ligand charge transfer (350–470 nm), respectively (Fig. S10, SI). Upon 405 nm excitation, both **Ir1** and **Ir2** exhibited intensive emission centered at 605 nm (Fig. S11, SI). All photophysical data are listed in Table S1. It was found that the emissive intensity of **Ir1** was sensitive to pH values 3.0–8.0; the more acidic the environment the stronger the emission intensity (Fig. S11, SI). This was due to protonation of the imidazole ring on **Ir1**. Such pH-dependent luminescence changes were not obvious for **Ir2**. Considering the potential of adjacent imidazole and thiophene groups to bind zinc ions,²⁵ we also investigated the Zn²⁺ binding ability of **Ir1**/**Ir2** using NMR spectroscopy. ¹H NMR spectra showed that upon Zn²⁺ titration, the signals of both **Ir1** and **Ir2** at q, t, s, v, r, and y positions displayed a substantial shift to a high-field while the shift of **Ir1** was more prominent (Fig. 1). This indicated that **Ir1** and **Ir2** bound to Zn²⁺ mainly through the imidazole N atom and thiophene S atom, while the methyl substitution on the imidazole ring could weaken but not eliminate the Zn²⁺ binding ability. This moderate affinity may be more in line with our purpose of interfering with intracellular Zn²⁺ homeostasis through reversible binding and dissociation of metal ions, rather than tightly chelating metal ions which may transport extracellular Zn²⁺ from serum into cells, directly leading to the instability of many zinc-requiring enzymes.



Scheme 1 Chemical structures of designed Ir complexes in this work and their proposed mechanism of action. Mitochondria-targeted **Ir2** can modulate the homeostasis and distribution of endogenous zinc contents in both cancer cells and macrophages, thus effectively activating antitumour immunity.

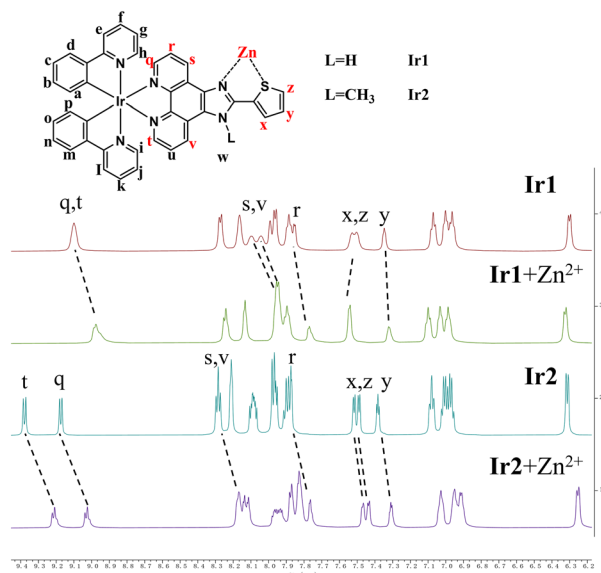


Fig. 1 Zinc titration: changes in the 600 MHz ^1H NMR spectra of **Ir1** and **Ir2** before and after the addition of Zn^{2+} in $\text{DMSO}-d_6$.

Subcellular localization of Ir complexes and re-distribution of endogenous zinc in mitochondria in MDA-MB-231 cells

Due to the excellent photophysical properties of Ir(III) complexes, their cellular uptake and distribution can be easily monitored by laser scanning confocal microscopy. It was observed that **Ir1**/**Ir2** could effectively penetrate into MDA-MB-231 cells in 1 h. Moreover, **Ir1** mainly accumulated in lysosomes while **Ir2** mainly accumulated in mitochondria, which exhibited strong colocalization with lysosome-specific and mitochondria-specific stains (LTDR and MTDR) with Pearson's correlation coefficients of 0.88 and 0.86, respectively (Fig. 2A). Meanwhile, the ability of **Ir1** and **Ir2** to regulate the distribution of intracellular Zn^{2+} was investigated in MDA-MB-231 cells by using ICP-MS. Herein, mitochondrial protein samples of MDA-MB-231 cells were measured by western blotting at equal concentrations, with VDAC and vinculin serving as markers of mitochondrial purity. As shown in Fig. S12, vinculin was negligible in complete mitochondria samples, implying that the purity of the mitochondria is sufficiently high (VDAC: Voltage-Dependent Anion Channel, residing in the outer mitochondrial membrane and serving as a standard mitochondrial marker protein; vinculin: cytoskeletal protein, not present in mitochondria and commonly used as a negative control for assessing mitochondrial purity). As shown in Fig. 2B, after the same treatment with **Ir1** and **Ir2** (5 μM , 8 h) in MDA-MB-231 cells, the total levels of intracellular zinc content were not substantially affected; however, the zinc content in the cytoplasm was found decreased accompanied by a significant increase in the mitochondria compared with control cells, and the effect of **Ir2** was more prominent.

Since **Ir1**/**Ir2** can decrease the zinc content in the cytoplasm accompanied by a significant increase in the mitochondria,

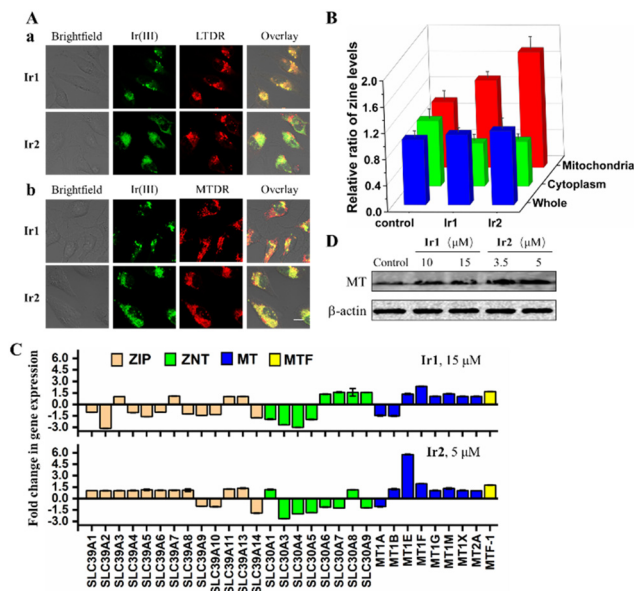


Fig. 2 (A) Cellular localization. The confocal microscopy images of MAD-MB-231 cells co-labeled with **Ir1**/**Ir2** (10 μM , 1 h, λ_{ex} = 405 nm and λ_{em} = 605 \pm 20 nm) and LTDR (50 nM, 0.5 h, λ_{ex} = 633 nm and λ_{em} = 665 \pm 25 nm) (a) or MTDR (150 nM, 0.5 h, λ_{ex} = 633 nm and λ_{em} = 665 \pm 25 nm) (b). Scale bars: 20 μm . (B) Manipulation of Zn distribution and homeostasis. The relative ratio of Zn levels in whole cells, cytoplasm and mitochondria after treatment with **Ir1** (5 μM) or **Ir2** (5 μM) for 8 h. (C). Zn regulatory protein related genes in MDA-MB-231 cells after **Ir1** (15 μM , 8 h) and **Ir2** (5 μM , 8 h) treatment. (D) The expression of MT protein was measured by western blotting assay.

the effect of **Ir1**/**Ir2** on proteins that maintain Zn^{2+} homeostasis in MDA-MB-231 cells was also investigated by quantitative real-time polymerase chain reaction (RT-qPCR) measurements. Compared with control cells, metallothionein (MT) for Zn^{2+} buffering and storage was substantially up-regulated at the RNA level in **Ir2**-treated cells (fold change of *ca.* 5.7), which was much higher than that in **Ir1**-treated cells (fold change of *ca.* 2.4), indicating the more prominent ability of **Ir2** to regulate the intracellular Zn^{2+} level (Fig. 2C). The expression of MT protein was also measured by western blotting assay, showing that both **Ir1** and **Ir2** could upregulate the expression levels of MT protein in a dose-dependent manner, the latter of which showed a more prominent effect (Fig. 2D). These observations were consistent with the ICP-MS results in MDA-MB-231 cells, indicating that both **Ir1** and **Ir2** could re-distribute endogenous zinc contents, leading to their excess accumulation in mitochondria.

As a result, both **Ir1** and **Ir2** could induce mitochondrial dysfunction but to varying degrees. As shown in JC-1 staining assay, **Ir2** induced substantial loss of mitochondrial membrane potential (MMP) as indicated by the red-to-green colour shift of 5,5',6,6'-tetrachloro-1,1',3,3' tetraethylbenzimidazolylcarbocyanine iodide (JC-1), while **Ir1** only exhibited a small impact on MMP loss (Fig. 3A). Compared with vehicle-treated cells, both **Ir1** and **Ir2** could increase intra-

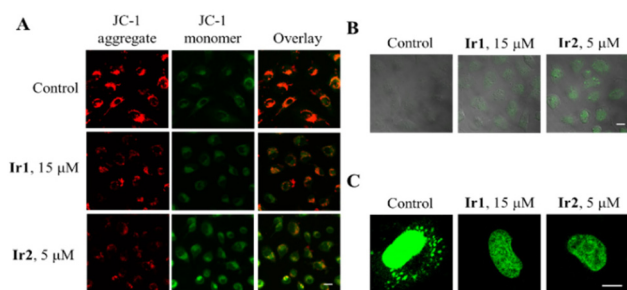


Fig. 3 Mitochondrial dysfunction (A), increasing the production of ROS (B) mitochondrial DNA damage (C) examined by confocal microscopy images after treatment with Ir1/Ir2 for 8 h. Scale bars: 20 μ m.

cellular ROS production as indicated by DCF fluorescence intensity, indicating greater production of ROS, and the effect of Ir2 was more prominent (Fig. 3B). Meanwhile, substantially diminished fluorescence from Pico-Green and acridine orange (AO) was observed in Ir1/Ir2-treated cells compared with that in control cells, indicating that both Ir1 and Ir2 could induce mitochondrial DNA damage and lysosomal impairment (Fig. 3C and Fig. S13). Among them, Ir2 displayed a more pronounced effect than Ir1, which was reasonable due to its better mitochondria targeting ability and mitochondrial zinc re-distribution.

Antiproliferative activity, pyroptosis induction and PD-L1 down-regulation in MDA-MB-231 cells

Furthermore, the effect of Ir1/Ir2 on programmed cell death and immune regulation was investigated. First, both Ir1 and Ir2 exhibited a high anti-proliferative effect against cancerous cell lines. As shown in 48 h MTT assay, the resulting IC₅₀ values of Ir1/Ir2 were in the range of 2.0–3.2 μ M, which were *ca.* 10-times smaller than that of cisplatin in cancerous cell. The related metal complexes Ir3 containing similar ligands without a Zn²⁺ binding moiety show weaker antiproliferative activity compared to Ir1/Ir2 (Table 1). Second, the effect of various cell death inhibitors on the viability of Ir1/Ir2 treated cells was investigated, showing that pre-incubation with apoptosis inhibitors (Z-VAD-fmk) could improve the viability of Ir1-treated cells while both Z-VAD-fmk and pyroptosis inhibitors (Disulfiram) could improve the viability of Ir2-treated cells

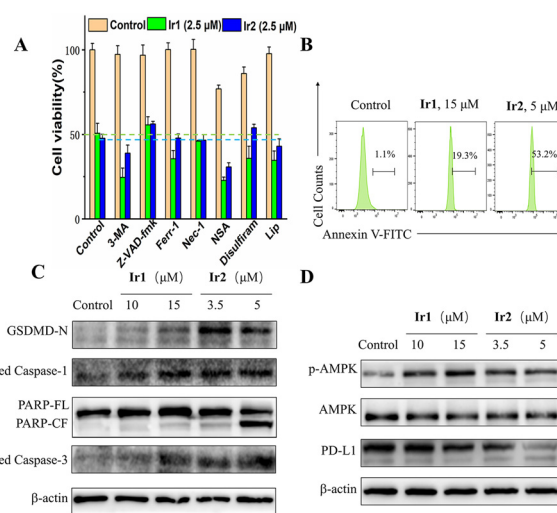


Fig. 4 Activation of anti-tumour immunity by triggering pyroptosis and down-regulating PD-L1 levels. (A) The effects of different inhibitors on cell death induced by Ir1/Ir2 for 48 h. (B) Flow-cytometric quantification of Annexin V-labeled cells after treatment with Ir1/Ir2 for 8 h. (C and D) Western blot analysis of cleaved caspase-1, GSDMD-N fragment, cleaved caspase-3, PARP, AMPK, p-AMPK, PD-L1 and β -actin upon 8 h treatment with compounds.

(Fig. 4A). Meanwhile, flow cytometry showed a substantial increase in Annexin V staining in Ir1/Ir2-treated cells, further indicating the occurrence of early apoptosis (Fig. 4B). Considering that disulfiram is a broad-spectrum thiol-reactive agent rather than a selective pyroptosis inhibitor,³⁴ we further measured the cleavage of caspase-1 and gasdermin D (GSDMD) as pyroptosis-specific protein markers. Western blotting assay showed that both Ir1 and Ir2 could upregulate the expression levels of caspase-1, cleaved caspase-1 and N-terminal fragment of GSDMD (GSDMD-N) in a dose-dependent manner, the latter of which showed a more prominent effect (Fig. 4C and Fig. S14). Moreover, apoptosis protein marker cleaved caspase 3 and PARP were also upregulated in response to Ir1/Ir2 treatment (Fig. 4C). These results indicated that both Ir1/Ir2 could induce caspase-3 dependent apoptosis and caspase-1 dependent GSDMD mediated pyroptosis, and the mitochondria-targeted Ir2 had a greater effect.

Table 1 IC₅₀ values of the tested compounds against different cell lines against cancerous (MDA-MB-231, A549, HeLa and 4T1) and normal breast cell (MCF-10A) lines for 48 h^a

| Compounds | IC ₅₀ (μ M) | | | | |
|-----------|-----------------------------|----------------|----------------|----------------|----------------|
| | MDA-MB-231 | A549 | HeLa | 4T1 | MCF-10A |
| Ir1 | 2.3 \pm 0.1 | 3.2 \pm 0.2 | 2.2 \pm 0.6 | 2.4 \pm 0.1 | 5.1 \pm 0.3 |
| Ir2 | 2.0 \pm 0.2 | 3.1 \pm 0.3 | 2.1 \pm 0.2 | 1.1 \pm 0.1 | 3.7 \pm 0.2 |
| Ir3 | 3.1 \pm 0.3 | 4.7 \pm 0.2 | 4.1 \pm 0.2 | 4.9 \pm 0.2 | 5.6 \pm 0.5 |
| Cisplatin | 35.8 \pm 1.9 | 21.8 \pm 1.4 | 18.3 \pm 0.8 | 21.8 \pm 0.4 | 30.9 \pm 0.6 |

^a IC₅₀ values are drug concentrations necessary for 50% inhibition of cell viability. Data are presented as means \pm standard deviations obtained in at least three independent experiments and the drug treatment period was 48 h.

Considering that interference with mitochondria metabolism could activate adenosine 5'-monophosphate-activated protein kinase (AMPK), which is a promising PD-L1 regulator,^{35–37} we also measured the PD-L1 levels in **Ir1**/**Ir2** treated cancer cells by western blot assay. As shown in Fig. 4D, the expression level of intracellular PD-L1 was found markedly down-regulated accompanied by the up-regulation of p-AMPK in response to **Ir2** treatment (3.5–5 μM , 8 h); however, PD-L1 down-regulation was not significant after **Ir1** treatment at high doses (10–15 μM). According to the literature, activation of AMPK can not only phosphorylate PD-L1 at S195 to induce abnormal glycosylation and degradation of PD-L1 through an endoplasmic reticulum associated proteasome degradation (ERAD) pathway,³⁵ but also facilitate the nuclear translocation of TFEB and lysosome biogenesis *via* mTOR inhibition for lysosomal degradation of PD-L1.^{38,39} We found that the expression level of mTOR/p-mTOR, a downstream protein of the AMPK signalling pathway, also decreased after **Ir1**/**Ir2** treatment in MDA-MB-231 cells, and **Ir2** showed a more prominent effect (Fig. S15, SI). Considering that both **Ir1** and **Ir2** could induce lysosomal impairment as indicated by the acridine orange (AO) staining (Fig. S13), the capability of **Ir1**/**Ir2** to down-regulate PD-L1 levels is mainly through an AMPK mediated ERAD pathway rather than the AMPK mediated lysosomal degradation pathway. On the other hand, we also evaluated the expression level of STAT3/p-STAT3, the inactivation of which could also down-regulate PD-L1 levels.^{40,41} As shown in Fig. S16, the expression level of intracellular STAT3/p-STAT3 was found to show no substantial changes in response to **Ir1**/**Ir2** treatment, excluding the STAT3 mediated PD-L1 down-regulation in **Ir1**/**Ir2** treated cells. Besides, the expression level of GSDMD-N was not upregulated and PD-L1 down-regulation was not significant after **Ir3** treatment at high-doses (10–15 μM) (Fig. S17). These results showed that mitochondria-targeted **Ir2** with intracellular zinc distribution/homeostasis regulation capability has the greatest potential to activate anti-tumor immune effects.

Subcellular localization of Ir complexes, re-distribution of endogenous zinc, and polarization of RAW 264.7 macrophages

We further investigated the effect of Ir complexes on macrophages. Laser scanning confocal microscopy of RAW 264.7 macrophages showed a similar phenomenon as observed in MDA-MB-231 cancer cells, where **Ir1** mainly accumulates in lysosomes and **Ir2** mainly accumulates in mitochondria (Fig. 5A). The ability of **Ir1** and **Ir2** to regulate the distribution of intracellular Zn^{2+} was further investigated in RAW 264.7 macrophages by using ICP-MS. In addition, mitochondrial protein samples of RAW 264.7 macrophages were measured by western blotting at equal concentrations, with VDAC and vinculin serving as markers of mitochondrial purity (VDAC: Voltage-Dependent Anion Channel, residing in the outer mitochondrial membrane, serving as a standard mitochondrial marker protein; vinculin: cytoskeletal protein, localized to focal adhesions and cell-cell junctions (not present in mitochondria), used as a negative control marker to assess

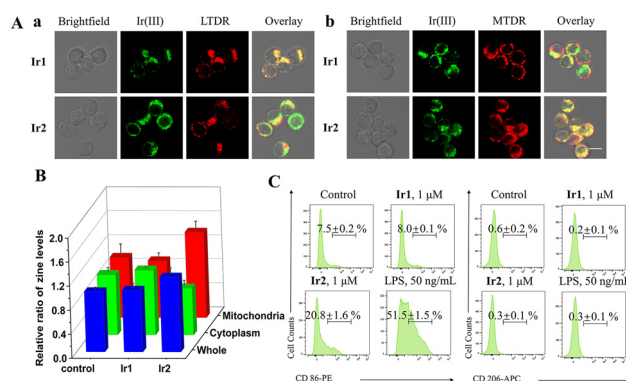


Fig. 5 (A) Cellular localization. The confocal microscopy images of RAW 264.7 macrophages co-labeled with **Ir1**/**Ir2** (10 μM , 1 h, λ_{ex} = 405 nm and λ_{em} = 605 \pm 20 nm) and LTDR (50 nM, 0.5 h, λ_{ex} = 633 nm and λ_{em} = 665 \pm 25 nm) (a) or MTDR (150 nM, 0.5 h, λ_{ex} = 633 nm and λ_{em} = 665 \pm 25 nm) (b). Scale bars: 20 μm . (B) Manipulation of Zn distribution and homeostasis. The relative ratio of Zn levels in whole cells, cytoplasm and mitochondria after treatment with **Ir1** (1 μM) or **Ir2** (1 μM) for 48 h. (C) Flow cytometry analyses of the representative receptors CD 86 of M1 macrophages (a) or CD 206 of M2 macrophages (b).

mitochondrial purity). As shown in Fig. S18, vinculin was negligible in complete mitochondria samples, implying that the purity of the mitochondria is sufficiently high. On treatment with **Ir1** (1 μM , 48 h) in RAW 264.7 macrophages, the levels of zinc content in whole cell, cytoplasm and mitochondria were not substantially affected. However, on treatment with **Ir2** (1 μM , 48 h) in RAW 264.7 macrophages, the levels of zinc content in whole cells and mitochondria were found to increase accompanied by a decrease in the cytoplasm compared with that of control cells (Fig. 5B). The different distributions of Zn content on macrophage treatment with **Ir1** and **Ir2** may cause varying degrees of polarization from M0 to M1 in macrophages.

Considering that zinc supplementation can promote M0-to-M1 polarization of macrophages and inhibit M2 polarization,⁹ the effect of Ir complexes on macrophage polarization was also investigated. As shown in flow cytometry assay, after **Ir2** (0.5–1 μM , 48 h) treatment, the pro-inflammatory M1 phenotype marked by CD86 remarkably increased (control: 7.3%; **Ir2**, 0.5 μM : 12.2%; 1 μM : 21.9%) in a concentration-dependent manner (Fig. 5Ca and S19, 20). Meanwhile, the M2 phenotype marked by CD206 was not affected in response to **Ir2** treatment under the same conditions (Fig. 5Cb). By comparison, neither M0-to-M1 nor M0-to-M2 polarization was affected in response to **Ir1** treatment (Fig. 5C). These observations were consistent with the ICP-MS results of the distribution of Zn^{2+} in macrophages, indicating that **Ir2** could effectively re-distribute endogenous zinc contents, leading to their excess accumulation in mitochondria. These results indicated that **Ir2** had great potential to activate anti-tumour immunity by triggering cancer cell pyroptosis, down-regulating PD-L1 levels and promoting the polarization of macrophages from the M0 to the M1 phenotype.

Antitumor efficacy and antitumor immunity *in vivo*

To evaluate the anti-tumor efficacy and capability to activate immune responses of cyclometalated Ir(III) complexes *in vivo*, we established the immunocompetent mouse breast cancer (4T1) subcutaneous bearing bilateral model upon female BALB/C mice. 4T1 cells were inoculated to the right flank of mice as primary tumors and the left flank as distant tumors 7 days later. Cisplatin, **Ir1** and **Ir2** (3 mg kg^{-1}), respectively, were intratumorally injected into the primary tumors. The volumes of both primary and distant tumors as well as the mouse weights were measured every 2 days, and the mice were sacrificed at the 14th day (Fig. 6A). The body weights of all groups remained stable during the therapeutic process (Fig. 6B), and no structural or pathological changes occurred in the major organs (liver, heart, lungs, kidneys, and spleen) as revealed by hematoxylin and eosin (H&E) staining at the end of the treatment (Fig. S21 and S22). Meanwhile, the volume of primary tumors was inhibited by 50.5% in **Ir2**-treated groups, while cis-

platin and **Ir1** inhibited the tumor growth by 32.2% and 36.9%, respectively (Fig. 6C and S23). Additionally, the growth of distant tumors in **Ir2**-treated groups was significantly inhibited by 46.1% compared with that in the control group, but no obvious inhibition effect was found in the cisplatin or **Ir1** groups (Fig. 6D and S23).

Then the ability of **Ir2** to activate antitumor immunity *in vivo* was evaluated by profiling the infiltration of immune cells *in vivo*. It was found that the macrophage polarization and maturation of dendritic cells (DC) in primary tumors were greatly promoted by **Ir2**, as indicated by the significantly increased percentage of tumor-associated M1 macrophages (from 6.2% to 13.8%) and increased percentage of $\text{CD80}^+\text{CD86}^+$ DCs (from 4.5% to 15.9%) (Fig. 6E and S24, S25). Meanwhile, the infiltration of cytotoxic and helper T cells were found to be substantially enhanced in the **Ir2** group compared with that in the control group, as indicated by the increased proportion of tumor-infiltrating $\text{CD3}^+\text{CD4}^+$ (from 3.0% to 7.4%) and $\text{CD3}^+\text{CD8}^+$ T lymphocytes (from 2.9% to 7.1%), respectively (Fig. 6E and S26, S27). Meanwhile, immunohisto-fluorescence analysis in distant tumors was also performed, both of which showed enhanced tumor-associated M1 macrophages and tumor-infiltrating $\text{CD3}^+\text{CD8}^+$ in the **Ir2** group compared with control groups (Fig. 6F and S28). We also evaluated the ability of **Ir2** to reduce PD-L1 protein levels *in vivo* using immunohistochemistry (Fig. 6G). Compared with the control group, the expression level of PD-L1 in tumor tissues was slightly upregulated in the cisplatin group but significantly decreased in the **Ir2** group, verifying the ability of **Ir2** to down-regulate the PD-L1 levels in tumors. Furthermore, the enzyme-linked immunosorbent assay (ELISA) showed increased levels of the proinflammatory cytokines Interferon- β (IFN- β) and TNF- α in serum samples from **Ir2** groups, while minimal changes were observed in other groups (Fig. S29). In short, all these results verified that **Ir2** could not only inhibit tumor growth but also act as a small molecular inhibitor of PD-L1, eventually achieving immunochemotherapy *in vivo*.

Conclusions

In summary, we have developed two cyclometalated Ir(III) complexes (**Ir1** and **Ir2**) with moderate Zn^{2+} affinity, capable of redistributing the endogenous zinc from cytoplasm and vesicles to mitochondria, which leads to excess Zn^{2+} accumulation in the mitochondria of cancer cells. This change in the distribution of Zn^{2+} ions in macrophages was only found in **Ir2**. Although **Ir1** and **Ir2** show similar anti-proliferative activity on cancer cells, the mitochondria-targeted **Ir2** has a more prominent effect on regulating zinc homeostasis, thus effectively triggering GSDMD-mediated pyroptosis, down-regulating PD-L1 expression, promoting macrophage M0-to-M1 polarization, and activating anti-tumor immunity *in vivo*, eventually showing great potential in cancer chemo-immunotherapy. This work indicates that modulating the homeostasis and distribution of endogenous zinc will help activate antitumour

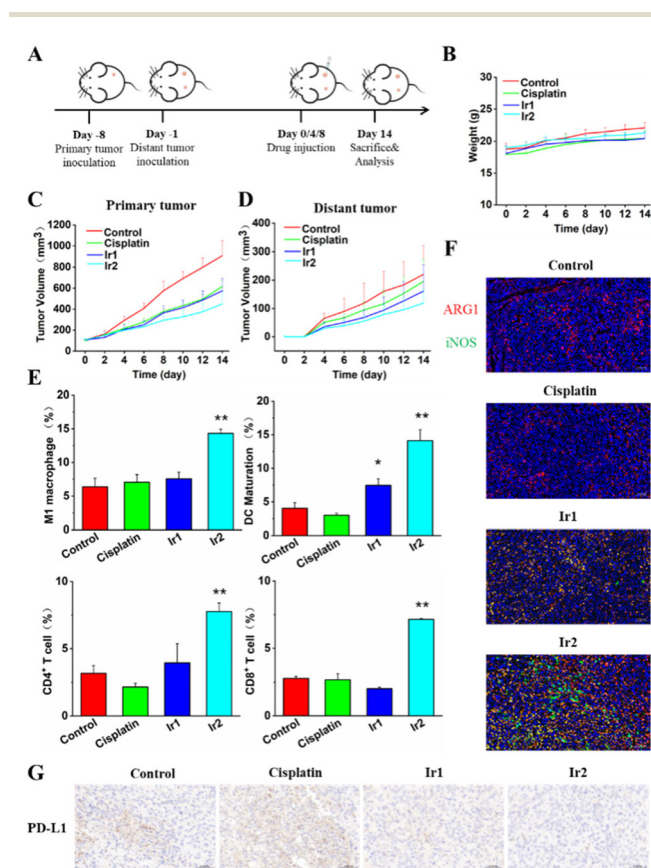


Fig. 6 *In vivo* antitumor efficacy and antitumor immune response. (A) Schematic illustration of the *in vivo* therapeutic schedule of the bilateral tumor model. (B) The weight of the mice during the treatment. (C and D) The curves of the volume of primary and distant tumors. (E) Data statistics of the $\text{CD80}^+\text{CD86}^+$ dendritic cells, CD4^+ T cells, CD8^+ T cells and M1 macrophage cells in tumor cells after different treatments ($n = 3$). (F) Immunofluorescence of ARG1 (M2 macrophages) and iNOS (M1 macrophages) in distant tumors from mice with different treatments of the bilateral tumor model. (G) IHC analysis of PD-L1 in tumor tissues. $^*p < 0.05$ and $^{**}p < 0.01$.

immunity, providing new clues for the development of novel metal-based anticancer complexes.

Author contributions

JJL and XSF contributed equally to this work. JJL, ZWM and QC conceived this study and designed the experiments. JJL, XSF, YL, and WDC completed material synthesis, characterization and data analysis. JJL, XSF, and YL contributed to cellular studies. JJL, XSF and QC contributed to the data analysis and wrote the manuscript. QC and ZWM provided the funds to support this article. All authors revised this manuscript. All animal experiments were approved by the Institutional Animal Care and Use Committee (IACUC), Sun Yat-Sen University (Approval No.: SYSU-IACUC 2024-B1561). SPF female BALB/c mice ($n = 20$), 5–6 weeks of age, were purchased from Guangdong Provincial Medical Laboratory Animal Center and bred in the Experimental Animal Center of Sun Yat-Sen University. After 7 days of adaptive feeding, the mice were 6–7 weeks old and had body weights of 20.6 ± 1.1 g at the time of the *in vivo* antitumor experiments.

Conflicts of interest

There are no conflicts to declare.

Data availability

The data supporting this article have been included as part of the SI.

Supplementary information is available. Additional experimental details, materials, and methods. See DOI: <https://doi.org/10.1039/d5dt01045d>.

Acknowledgements

We are grateful for financial support from the National Natural Science Foundation of China [22177141, 22371305, and 92353301], Guangdong Basic and Applied Basic Research Foundation [2024A1515010770], and Fundamental Research Funds for the Central Universities [87000-31670001].

References

- 1 E. Bafaro, Y. Liu, Y. Xu and R. E. Dempsey, The emerging role of zinc transporters in cellular homeostasis and cancer, *Signal Transduction Targeted Ther.*, 2017, **2**, 17029.
- 2 W. Maret, Zinc biochemistry: from a single zinc enzyme to a key element of life, *Adv. Nutr.*, 2013, **4**, 82–91.
- 3 M. I. Costa, A. B. Sarmiento-Ribeiro and A. C. Gonçalves, Zinc: From Biological Functions to Therapeutic Potential, *Int. J. Mol. Sci.*, 2023, **24**, 4822.
- 4 D. D. Marreiro, K. J. Cruz, J. B. Morais, J. B. Beserra, J. S. Severo and A. R. de Oliveira, Zinc and Oxidative Stress: Current Mechanisms, *Antioxidants*, 2017, **6**, 24.
- 5 Y. Yang, H. H. Fan, X. Y. Xu, S. K. Yao, W. H. Yu and Z. J. Guo, Zinc Ion-Induced Immune Responses in Antitumor Immunotherapy, *CCS Chem.*, 2024, **6**, 2210–2229.
- 6 M. Du and Z. J. Chen, DNA-induced liquid phase condensation of cGAS activates innate immune signaling, *Science*, 2018, **361**, 704–709.
- 7 S. F. Yang, C. B. Nelson, J. K. Wells, M. Fernando, R. Lu, J. A. M. Allen, L. Malloy, N. Lamm, V. J. Murphy, J. P. Mackay, A. J. Deans, A. J. Cesare, A. P. Sobinoff and H. A. Pickett, ZNF827 is a single-stranded DNA binding protein that regulates the ATR-Chk1 DNA damage response pathway, *Nat. Commun.*, 2024, **15**, 2210.
- 8 H. Gao, L. Zhao, H. Wang, E. Xie, X. Wang, Q. Wu, Y. Yu, X. He, H. Ji, L. Rink, J. Min and F. Wang, Metal transporter SLC39A10 regulates susceptibility to inflammatory stimuli by controlling macrophage survival, *Proc. Natl. Acad. Sci. U. S. A.*, 2017, **114**, 12940–12945.
- 9 L. Dierichs, V. Kloubert and L. Rink, Cellular zinc homeostasis modulates polarization of THP-1-derived macrophages, *Eur. J. Nutr.*, 2018, **57**, 2161–2169.
- 10 D. Yang, T. Tian, X. Li, B. Zhang, L. Qi, F. Zhang, M. Han, S. Wang, J. Xiao, Y. Gou, R. Zhang, Q. Liu, S. Su, J. Liu, X. Huang, Q. Gao, L. Hui, H. Tang, Y. Chen, H. Wang and B. Wei, ZNT1 and Zn^{2+} control TLR4 and PD-L1 endocytosis in macrophages to improve chemotherapy efficacy against liver tumor, *Hepatology*, 2024, **80**, 312–329.
- 11 X. Sun, X. Zhou, X. Shi, O. A. Abed, X. An, Y. L. Lei and J. J. Moon, Strategies for the development of metalloimmunotherapies, *Nat. Biomed. Eng.*, 2024, **8**, 1073–1091.
- 12 S. Chen, A. Saeed, Q. Liu, Q. Jiang, H. Xu, G. G. Xiao, L. Rao and Y. Duo, Macrophages in immunoregulation and therapeutics, *Signal Transduction Targeted Ther.*, 2023, **8**, 207.
- 13 Y. N. Chen, M. R. Hu, L. Wang and W. D. Chen, Macrophage M1/M2 polarization, *Eur. J. Pharmacol.*, 2020, **877**, 173090.
- 14 J. Liu, X. Geng, J. Hou and G. Wu, New insights into M1/M2 macrophages: key modulators in cancer progression, *Cancer Cell Int.*, 2021, **21**, 389.
- 15 X. Sun, Y. Zhang, J. Li, K. S. Park, K. Han, X. Zhou, Y. Xu, J. Nam, J. Xu, X. Shi, L. Wei, Y. L. Lei and J. J. Moon, Amplifying STING activation by cyclic dinucleotide-manganese particles for local and systemic cancer metalloimmunotherapy, *Nat. Nanotechnol.*, 2021, **16**, 1260–1270.
- 16 N. Toupin, M. K. Herroon, R. P. Thummel, C. Turro, I. Podgorski, H. Gibson and J. J. Kodanko, Metalloimmunotherapy with Rhodium and Ruthenium Complexes: Targeting Tumor-Associated Macrophages, *Chem. – Eur. J.*, 2022, **28**, e202104430.
- 17 C. Wang, R. Zhang, X. Wei, M. Lv and Z. Jiang, Metalloimmunology: The metal ion-controlled immunity, *Adv. Immunol.*, 2020, **145**, 187–241.

- 18 C. Yang, Y. Luo, H. Shen, M. Ge, J. Tang, Q. Wang, H. Lin, J. Shi and X. Zhang, Inorganic nanosheets facilitate humoral immunity against medical implant infections by modulating immune co-stimulatory pathways, *Nat. Commun.*, 2022, **13**, 4866.
- 19 H. Jiang, Y. Guo, C. Wei, P. Hu and J. Shi, Nanocatalytic Innate Immunity Activation by Mitochondrial DNA Oxidative Damage for Tumor-Specific Therapy, *Adv. Mater.*, 2021, **33**, e2008065.
- 20 Y. Yang, Y. F. Zhu, K. R. Wang, Y. Q. Miao, Y. Y. Zhang, J. Gao, H. L. Qin and Y. Zhang, Activation of autophagy by in situ Zn^{2+} chelation reaction for enhanced tumor chemioimmunotherapy, *Bioact. Mater.*, 2023, **29**, 116–131.
- 21 D. Cen, Q. Ge, C. Xie, Q. Zheng, J. Guo, Y. Zhang, Y. Wang, X. Li, Z. Gu and X. Cai, ZnS@BSA Nanoclusters Potentiate Efficacy of Cancer Immunotherapy, *Adv. Mater.*, 2021, **33**, e2104037.
- 22 L. Sun, H. B. Gao, H. Wang, J. W. Zhou, X. R. Ji, Y. X. Jiao, X. J. Qin, D. L. Ni and X. P. Zheng, Nanoscale Metal-Organic Frameworks-Mediated Degradation of Mutant p53 Proteins and Activation of cGAS-STING Pathway for Enhanced Cancer Immunotherapy, *Adv. Sci.*, 2024, **11**, e2307278.
- 23 Y. Y. Wang, S. L. Li, X. Y. Zhang, F. L. Jiang, Q. L. Guo, P. Jiang and Y. Liu, “Multi-in-One” Yolk-Shell Structured Nanoplatfrom Inducing Pyroptosis and Antitumor Immune Response Through Cascade Reactions, *Small*, 2024, **20**, e2400254.
- 24 B. B. Ding, H. Chen, J. Tan, Q. Meng, P. Zheng, P. A. Ma and J. Lin, ZIF-8 Nanoparticles Evoke Pyroptosis for High-Efficiency Cancer Immunotherapy, *Angew. Chem., Int. Ed.*, 2023, **62**, e202215307.
- 25 X. X. Su, B. Liu, W. J. Wang, K. Peng, B. B. Liang, Y. Zheng, Q. Cao and Z. W. Mao, Disruption of Zinc Homeostasis by a Novel Platinum(IV)-Terthiophene Complex for Antitumor Immunity, *Angew. Chem., Int. Ed.*, 2023, **62**, e202216917.
- 26 V. Novohradsky, A. Marco, L. Markova, N. Cutillas, J. Ruiz and V. Brabec, Ir(III) Compounds Containing a Terdentate Ligand Are Potent Inhibitors of Proliferation and Effective Antimetastatic Agents in Aggressive Triple-Negative Breast Cancer Cells, *J. Med. Chem.*, 2023, **66**, 9766–9783.
- 27 J. Sanz-Villafruela, C. Bermejo-Casadesus, E. Zafon, M. Martínez-Alonso, G. Durá, A. Heras, I. Soriano-Díaz, A. Giussani, E. Ortí, F. Tebar, G. Espino and A. Massaguer, Insights into the anticancer photodynamic activity of Ir(III) and Ru(II) polypyridyl complexes bearing β -carboline ligands, *Eur. J. Med. Chem.*, 2024, **276**, 116618.
- 28 H. Shi, O. W. L. Carter, F. Ponte, C. Imberti, M. A. Gomez-Gonzalez, F. Cacho-Nerin, P. D. Quinn, J. E. Parker, E. Sicilia, H. Huang and P. J. Sadler, A Photodynamic and Photochemotherapeutic Platinum-Iridium Charge-Transfer Conjugate for Anticancer Therapy, *Angew. Chem., Int. Ed.*, 2024, **63**, e202400476.
- 29 M. D. Lv, Y. Zheng, J. Wu, Z. Q. Shen, B. L. Guo, G. J. Hu, Y. L. Huang, J. Y. Zhao, Y. Qian, Z. Su, C. Wu, X. L. Xue, H. K. Liu and Z. W. Mao, Evoking Ferroptosis by Synergistic Enhancement of a Cyclopentadienyl Iridium-Betulin Immune Agonist, *Angew. Chem., Int. Ed.*, 2023, **62**, e202312897.
- 30 D. Deng, M. Wang, Y. Su, H. Fang, Y. Chen and Z. Su, Iridium(III)-Based PD-L1 Agonist Regulates p62 and ATF3 for Enhanced Cancer Immunotherapy, *J. Med. Chem.*, 2024, **67**, 6810–6821.
- 31 L. Wang, J. Karges, F. Wei, L. Xie, Z. Chen, G. Gasser, L. Ji and H. Chao, mitochondria-localized iridium(III) photosensitizer for two-photon photodynamic immunotherapy against melanoma, *Chem. Sci.*, 2023, **14**, 1461–1471.
- 32 S. Sen, M. Won, M. S. Levine, Y. Noh, A. C. Sedgwick, J. S. Kim, J. L. Sessler and J. F. Arambula, Metal-based anti-cancer agents as immunogenic cell death inducers: the past, present, and future, *Chem. Soc. Rev.*, 2022, **51**, 1212–1233.
- 33 R. Cao, J. Jia, X. Ma, M. Zhou and H. Fei, Membrane localized iridium(III) complex induces endoplasmic reticulum stress and mitochondria-mediated apoptosis in human cancer cells, *J. Med. Chem.*, 2013, **56**, 3636–3644.
- 34 J. J. Hu, X. Liu, S. Xia, Z. Zhang, Y. Zhang, J. Zhao, J. Ruan, X. Luo, X. Lou, Y. Bai, J. Wang, L. R. Hollingsworth, V. G. Magupalli, L. Zhao, H. R. Luo, J. Kim, J. Lieberman and H. Wu, FDA-approved disulfiram inhibits pyroptosis by blocking gasdermin D pore formation, *Nat. Immunol.*, 2020, **21**, 736–745.
- 35 J. H. Cha, W. H. Yang, W. Xia, Y. Wei, L. C. Chan, S. O. Lim, C. W. Li, T. Kim, S. S. Chang, H. H. Lee, J. L. Hsu, H. L. Wang, C. W. Kuo, W. C. Chang, S. Hadad, C. A. Purdie, A. M. McCoy, S. Cai, Y. Tu, J. K. Litton, E. A. Mittendorf, S. L. Moulder, W. F. Symmans, A. M. Thompson, H. Piwnicka-Worms, C. H. Chen, K. H. Khoo and M. C. Hung, Metformin Promotes Antitumor Immunity via Endoplasmic-Reticulum-Associated Degradation of PD-L1, *Mol. Cell.*, 2018, **71**, 606–620.
- 36 Y. Liu, Z. Zhou, J. Hou, W. Xiong, H. Kim, J. Chen, C. Zheng, X. Jiang, J. Yoon and J. Shen, Tumor Selective Metabolic Reprogramming as a Prospective PD-L1 Depression Strategy to Reactivate Immunotherapy, *Adv. Mater.*, 2022, **34**, e2206121.
- 37 E. Q. Toyama, S. Herzig, J. Courchet, T. L. Lewis Jr., O. C. Losón, K. Hellberg, N. P. Young, H. Chen, F. Polleux, D. C. Chan and R. J. Shaw, Metabolism. AMP-activated protein kinase mediates mitochondrial fission in response to energy stress, *Science*, 2016, **351**, 275–281.
- 38 X. Liu, M. Yin, J. Dong, G. Mao, W. Min, Z. Kuang, P. Yang, L. Liu, N. Zhang and H. Deng, Tubeimoside-1 induces TFEB-dependent lysosomal degradation of PD-L1 and promotes antitumor immunity by targeting mTOR, *Acta Pharm. Sin. B*, 2021, **11**, 3134–3149.
- 39 N. Malik, B. I. Ferreira, P. E. Hollstein, S. D. Curtis, E. Trefts, S. Weiser Novak, J. Yu, R. Gilson, K. Hellberg, L. Fang, A. Sheridan, N. Hah, G. S. Shadel, U. Manor and R. J. Shaw, Induction of lysosomal and mitochondrial biogenesis by AMPK phosphorylation of FNIP1, *Science*, 2023, **380**, eabj5559.

- 40 T. L. Song, M. L. Nairismägi, Y. Laurensia, J. Q. Lim, J. Tan, Z. M. Li, W. L. Pang, A. Kizhakeyil, G. C. Wijaya, D. C. Huang, S. Nagarajan, B. K. Chia, D. Cheah, Y. H. Liu, F. Zhang, H. L. Rao, T. Tang, E. K. Wong, J. X. Bei, J. Iqbal, N. F. Grigoropoulos, S. B. Ng, W. J. Chng, B. T. Teh, S. Y. Tan, N. K. Verma, H. Fan, S. T. Lim and C. K. Ong, Oncogenic activation of the STAT3 pathway drives PD-L1 expression in natural killer/T-cell lymphoma, *Blood*, 2018, **132**, 1146–1158.
- 41 I. Zerdes, M. Wallerius, E. G. Sifakis, T. Wallmann, S. Betts, M. Bartish, N. Tsesmetzis, N. P. Tobin, C. Coucoravas, J. Bergh, G. Z. Rassidakis, C. Rolny and T. Foukakis, STAT3 Activity Promotes Programmed-Death Ligand 1 Expression and Suppresses Immune Responses in Breast Cancer, *Cancers*, 2019, **11**, 1479.